

Comparison of topological classifications of quadratic bosonic excitations with examples

Yan He¹ and Chih-Chun Chien²

¹*College of Physics, Sichuan University, Chengdu, Sichuan 610064, China**

²*Department of physics, University of California, Merced, CA 95343, USA.†*

The topological classifications of quadratic bosonic systems according to the symmetries of the dynamic matrices from the equations of motion of closed systems and the effective Hamiltonians from the Lindblad equations of open systems are summarized. The Hermitian bosonic Hamiltonians react to some symmetries differently from their fermionic counterparts. While the non-Hermitian dynamic matrix and effective Hamiltonian both lead to a ten-fold way table, the system-reservoir coupling may cause a system with or without coupling to a reservoir to fall into different classes. We present a 1D bosonic pairing model inspired by the fermionic Kitaev chain to contrast the topological behavior from the dynamic matrix and effective Hamiltonian. In contrast, a 2D Chern insulator is insensitive to the different classifications. Moreover, system-reservoir coupling may break time-reversal symmetry and cause the dynamic matrix and effective Hamiltonian of a bosonic time-reversal invariant topological insulator to fall into different classes.

I. INTRODUCTION

Studies of topological insulators and topological superconductors according to the underlying symmetries have led to “periodic tables” that classify various topological systems in different dimensions (see Refs. [1, 2] for a review). For electronic systems, the topological properties are usually analyzed by the band structures because the Fermi-Dirac statistics leads to occupied or unoccupied bands. Since the ground states of bosonic systems correspond to a Bose-Einstein condensate (BEC) of massive bosons or vacuum of massless bosons, topological properties of bosonic systems may be studied in the excited states via the Bogoliubov-de Gennes (BdG) formalism, which has been applied to collective modes of superfluid helium [3] and atomic BEC [4–7], photonics [8], phononics [9], magnons [10–12], magnetoelastic excitations [13], and others [14–17].

Subtle differences may arise in the classifications according to symmetries as different physical quantities may be chosen to examine the effects of symmetries. For instance, the Hamiltonians of isolated fermionic and bosonic systems react to the particle-hole symmetry differently [18, 19]. Due to the Bose-Einstein statistics, the BdG Hamiltonian and the equation of motion of bosonic excitations may react to a symmetry differently [18–21]. In contrast, the fermion BdG equation does not show such a complication. Explicitly, the time evolution of bosonic excitations follows a non-Hermitian dynamic matrix instead of the Hermitian Hamiltonian due to the underlying commutation relations. Moreover, non-Hermitian properties may be present even when the bosonic Hamiltonian is Hermitian [22]. Under certain conditions, the dynamics of quadratic bosonic systems may be mapped to more complicated fermionic sys-

tems [19, 20].

The second-quantized Hamiltonian of a quadratic fermionic (bosonic) system can be diagonalized by a Bogoliubov transformation with the coefficients forming a unitary (para-unitary) matrix in order to satisfy the anti-commutation (commutation) relations [3]. For bosons, the energy spectrum can be found equivalently from the diagonalization of the dynamic matrix [12, 14]. Importantly, the bosonic dynamic matrix transforms under the particle-hole symmetry in the same way as the fermionic Hamiltonian. Therefore, the tenfold-way classification of fermions applies to bosonic excitations according to their dynamic matrix, despite its non-Hermitian property. Interesting topological properties and invariants of non-Hermitian systems have been reviewed in Refs. [21, 23].

For quantum systems coupled to external reservoirs, the Lindblad equation has been widely used to describe quantum dynamics of open systems [24–26]. There have been many studies of topological properties of open quantum systems [27–32]. By implementing a method known as the “third quantization” for quadratic fermionic systems [33], Ref. [34] provides a classification of the steady states of the Lindblad equation according to the symmetries. Since the third quantization for quadratic bosonic systems has been developed [35] as well, here we analyze the topological classification of open quadratic bosonic systems described by the Lindblad equation. The effective Hamiltonian from the Lindblad equation plays the role of the dynamic matrix in the equation of motion of an isolated system. While non-Hermitian properties will be encountered in the dynamic matrix and effective Hamiltonian of bosons, here we only consider models with real line gaps or models whose complex spectrum can be continuously deformed into some intervals on the real axis. With this constraint, we will not address the full extent of the 38-fold way classification of non-Hermitian models [36]. In our discussion, the symmetry classes of non-Hermitian models will be reminiscent of the ten-fold way classification of Hermitian fermionic models. The clas-

* heyanc@scu.edu.cn

† cchien5@ucmerced.edu

sification according to the effective Hamiltonian, interestingly, has the same table as the one according to the dynamic matrix. However, we will show that the system-reservoir coupling of the Lindblad equation can introduce additional subtleties.

By analyzing concrete examples, we will show that bosonic systems may or may not exhibit different topological classifications according to the dynamic matrix, effective Hamiltonian, and their fermionic counterparts. Our 1D example is a bosonic pairing model with both s-wave and d-wave pairings. This is in contrast to the fermionic Kitaev chain [37] with p-wave pairing due to the Pauli exclusion principle. For the 1D bosonic pairing model, the classifications of the dynamic matrix and effective Hamiltonian agree if the system-reservoir coupling respects the particle-hole symmetry. In that case, the system shows a quantized Berry phase with periodic boundary condition and localized edge states with open boundary condition. However, if the system-reservoir coupling breaks the particle-hole symmetry, the effective Hamiltonian may belong to a different class from the one of the dynamic matrix. We also present a 2D bosonic Chern insulator that lacks a symmetry, therefore showing similar topological behavior according to different classifications. Our last example is the 2D time-reversal invariant topological insulator described by the four-band Bernevig-Hughes-Zhang (BHZ) model [38]. For the fermionic BHZ model, the topological properties have been demonstrated in semiconductor quantum wells [39]. We construct a bosonic version similar to that studied in Ref. [7] but consider both closed and open systems. A comparison shows that in the presence of Lindblad operators breaking time-reversal symmetry, the effective Hamiltonian from the Lindblad equation falls into a different class compared to the dynamic matrix of the bosonic BHZ model.

The rest of the paper is organized as follows. Sec. II summarizes the classifications of quadratic bosonic systems via symmetries and dimensions. The ten-fold way table according to the dynamic matrix from the equation of motion or the effective Hamiltonian from the Lindblad equation are explained. To contrast the difference, Sec. III shows a 1D bosonic pairing model that exhibits different topological behavior according to the different classifications. A 2D bosonic Chern insulator that does not differentiate the various classifications is also discussed. A 2D bosonic BHZ model shows how time-reversal symmetry breaking from Lindblad operators leads to different classes. Sec. IV concludes our work. In the Appendix, we summarize some details and subtleties.

II. SYMMETRIES AND CLASSIFICATIONS OF QUADRATIC BOSONIC SYSTEMS

A. Symmetries according to Hamiltonian

We begin by briefly reviewing the effects of symmetries on quadratic bosonic systems according to their Hamiltonians. The generic Hermitian Hamiltonian may be written in the BdG form as

$$\mathcal{H} = \sum_{a,b} \psi_a^\dagger H_{ab} \psi_b, \quad H = \begin{pmatrix} A & B \\ B^* & A^* \end{pmatrix}. \quad (1)$$

Here we define $\psi = (a_1, \dots, a_n, a_1^\dagger, \dots, a_n^\dagger)^T$. The matrices A and B satisfy $A^\dagger = A$ and $B^T = B$. The three types of symmetry conditions can be summarized [18] as

$$\text{Time-reversal:} \quad TH^*T^\dagger = H, \quad TT^* = \pm 1, \quad (2)$$

$$\text{Particle-hole:} \quad CH^*C^\dagger = H, \quad CC^* = \pm 1, \quad (3)$$

$$\text{Chiral or sublattice:} \quad SHS^\dagger = H, \quad S^2 = 1. \quad (4)$$

Here T , C and S are three unitary matrices that implement the three aforementioned symmetry conditions. Note that in the first-quantized form, the complex conjugation from time-reversal has already been imposed. The time reversal symmetry has the same effect on both bosonic and fermionic systems.

However, there are important differences in the particle-hole symmetry and chiral symmetry between bosonic and fermionic systems. For fermionic systems, we have

$$\text{Particle-hole:} \quad CH^*C^\dagger = -H, \quad CC^* = \pm 1, \quad (5)$$

$$\text{Chiral or sublattice:} \quad SHS^\dagger = -H, \quad S^2 = 1 \quad (6)$$

The minus sign on the right hand side of Eqs. (5) and (6) does not show up in the bosonic cases because of the commutation relations of bosonic operators. The chiral symmetry can be treated as a composition of the time-reversal and particle-hole symmetries. For fermions, it follows that $(CT)H(CT)^\dagger = -H$, where the minus sign comes from the particle-hole symmetry. For bosons, one instead obtains $(CT)H(CT)^\dagger = H$ without the minus sign. Details of the difference are summarized in the Appendix.

By treating the Hamiltonian as a mapping from the parameter space to a target space, a classification scheme has been developed [18]. As will be shown in the following, the more physically relevant classifications are according to the BdG structure. Thus, we leave the classification according the Hamiltonian to the Appendix.

B. Classification according to dynamic matrix

The dynamic matrix comes from the equation of motion of a quadratic bosonic system with the standard

commutation relation: ($\hbar \equiv 1$)

$$i \frac{d\psi_i}{dt} = [\psi_i, H] = \sum_j \left(\tau_3 H \right)_{ij} \psi_j. \quad (7)$$

Note that the boson operators satisfy the following canonical commutation relations:

$$[\psi_i, \psi_j^\dagger] = (\tau_3)_{ij}, \quad \psi = \left(a_1, \dots, a_n, a_1^\dagger, \dots, a_n^\dagger \right)^T. \quad (8)$$

Here we have introduced $\tau_i = \sigma_i \otimes I$, which applies to the "Nambu space" of bosons [7]. The dynamic matrix is given by

$$H_{\text{dyn}} = \tau_3 H = \begin{pmatrix} A & B \\ -B^* & -A^* \end{pmatrix}. \quad (9)$$

For fermionic systems, the dynamic matrix coincides with the Hamiltonian due to the fermionic anti-commutation relations. In the following, we will show that the dynamic matrix H_{dyn} of bosons may behave differently under symmetry transformations when compared to the Hermitian bosonic Hamiltonian H .

We apply the ideas of Refs. [34, 36] and use the three types of discrete symmetries to classify the dynamic matrix H_{dyn} of a quadratic boson system. We first discuss the time-reversal symmetry, under which the bosonic operators transform as

$$\mathcal{T} a_i \mathcal{T}^\dagger = \sum_j (T)_{ji} a_j, \quad \mathcal{T} a_i^\dagger \mathcal{T}^\dagger = \sum_j (T)_{ji}^* a_j^\dagger. \quad (10)$$

Here \mathcal{T} is the time-reversal operator in the second-quantization form. In the first-quantization form, the time-reversal symmetry of the Hamiltonian gives the condition

$$\begin{pmatrix} T & 0 \\ 0 & T^* \end{pmatrix}^\dagger \begin{pmatrix} A^* & B^* \\ B & A \end{pmatrix} \begin{pmatrix} T & 0 \\ 0 & T^* \end{pmatrix} = \begin{pmatrix} A & B \\ B^* & A^* \end{pmatrix}, \quad (11)$$

which in turn determines the transformations of the matrices A and B as

$$T^\dagger A^* T = A, \quad T^\dagger B^* T^* = B. \quad (12)$$

Then, the time-reversal of the dynamic matrix H_{dyn} is

$$\begin{pmatrix} T & 0 \\ 0 & T^* \end{pmatrix}^\dagger \begin{pmatrix} A^* & B^* \\ -B & -A \end{pmatrix} \begin{pmatrix} T & 0 \\ 0 & T^* \end{pmatrix} = \begin{pmatrix} A & B \\ -B^* & -A^* \end{pmatrix}. \quad (13)$$

Although H_{dyn} of a bosonic system may be non-Hermitian, it satisfies the time-reversal symmetry condition $T_1^\dagger H_{\text{dyn}}^* T_1 = H_{\text{dyn}}$ with $T_1 = \text{diag}(T, T^*)$. Therefore, the time-reversal symmetry of the dynamic matrix H_{dyn} of the bosonic system behaves just like a Hermitian fermionic Hamiltonian.

Next, we turn to the particle-hole symmetry of the dynamic matrix. Explicitly, the transformation matrix for the particle-hole symmetry may be taken as $C = \tau_1$, leading to

$$\tau_1 H_{\text{dyn}}^* \tau_1 = -H_{\text{dyn}}. \quad (14)$$

Class	T	C	S	$d=0$	$d=1$	$d=2$	$d=3$	$d=4$	$d=5$	$d=6$
A	0	0	0	\mathbb{Z}	0	\mathbb{Z}	0	\mathbb{Z}	0	\mathbb{Z}
AIII	0	0	1	0	\mathbb{Z}	0	\mathbb{Z}	0	\mathbb{Z}	0
AI	+	0	0	\mathbb{Z}	0	0	0	\mathbb{Z}	0	\mathbb{Z}_2
BDI	+	+	1	\mathbb{Z}_2	\mathbb{Z}	0	0	0	\mathbb{Z}	0
D	0	+	0	\mathbb{Z}_2	\mathbb{Z}_2	\mathbb{Z}	0	0	0	\mathbb{Z}
DIII	-	+	1	0	\mathbb{Z}_2	\mathbb{Z}_2	\mathbb{Z}	0	0	0
AII	-	0	0	\mathbb{Z}	0	\mathbb{Z}_2	\mathbb{Z}_2	\mathbb{Z}	0	0
CII	-	-	1	0	\mathbb{Z}	0	\mathbb{Z}_2	\mathbb{Z}_2	\mathbb{Z}	0
C	0	-	0	0	0	\mathbb{Z}	0	\mathbb{Z}_2	\mathbb{Z}_2	\mathbb{Z}
CI	+	-	1	0	0	0	\mathbb{Z}	0	\mathbb{Z}_2	\mathbb{Z}_2

Table I. Classification of symmetries and topology of quadratic bosonic systems according to their dynamic matrices. The first column shows the Cartan labels of the ten classes. The next three columns show the properties of these classes under time-reversal, particle-hole and chiral symmetries. Here 0 or 1 represents the absence or presence of the symmetry. The + and - signs correspond to $TT^* = \pm 1$ and $CC^* = \pm 1$. The last seven columns show the possible topological phases of the ten classes in various dimensions. The classification according to the effective Hamiltonian produces the same table, but the system-reservoir coupling may change which class a system belongs to.

Therefore, we arrived at the same particle-hole symmetry condition as a quadratic fermionic model. The composition of time-reversal and particle-hole symmetries gives rise to chiral symmetry. The condition $(CT)H_{\text{dyn}}(CT)^\dagger = -H_{\text{dyn}}$ behaves in the same way as the fermionic case does. In summary, for the non-Hermitian dynamic matrix H_{dyn} of bosons, the three discrete symmetry conditions are

$$\text{Time-reversal: } TH_{\text{dyn}}^* T^\dagger = H_{\text{dyn}}, \quad TT^* = \pm 1, \quad (15)$$

$$\text{Particle-hole: } CH_{\text{dyn}}^* C^\dagger = -H_{\text{dyn}}, \quad CC^* = \pm 1, \quad (16)$$

$$\text{Chiral or sublattice: } SH_{\text{dyn}} S^\dagger = -H_{\text{dyn}}, \quad S^2 = \mathbb{1} \quad (17)$$

Since the symmetry conditions are the same as the quadratic fermionic case, the ten-fold way classifications of quadratic fermionic systems [1] can be applied to the dynamic matrix of quadratic boson systems. The classification is summarized in Table I. We remark that particle-hole symmetry is only significant for systems with particle-hole mixing, which arises in systems with pairing effects. Therefore, models without particle-hole mixing do not discern the difference because particle-hole symmetry has no effect on them.

C. Classification according to effective Hamiltonian

We now turn to open quantum systems of bosons. The Lindblad quantum master equation for the time evolution of the reduced density matrix ρ under the influence of an environment with the Markovian approximation has the

expression [24–26] ($\hbar = 1$)

$$i\frac{d\rho}{dt} = \mathcal{L}(\rho) = [\mathcal{H}, \rho] + i \sum_{\mu} \left(2L_{\mu}\rho L_{\mu}^{\dagger} - \{L_{\mu}^{\dagger}L_{\mu}, \rho\} \right) \quad (18)$$

Here L_{μ} are the Lindblad operators modeling the environmental effects on the system. Assuming a quadratic bosonic system with n indices, the generic Hamiltonian is given by

$$\mathcal{H} = \sum_{i,j} \left(a_i^{\dagger} A_{ij} a_j + a_i A_{ij}^* a_j^{\dagger} + a_i B_{ij} a_j + a_i^{\dagger} B_{ij}^* a_j^{\dagger} \right) \quad (19)$$

Here the A and B satisfy $A^{\dagger} = A$ and $B^T = B$. To obtain an exact expression for classifying open bosonic systems, we consider linear Lindblad operators similar to those used in Ref. [35]:

$$L_{\mu} = \sum_j \left(l_{\mu j} a_j + k_{\mu j} a_j^{\dagger} \right). \quad (20)$$

We will focus on open systems that allow a steady-state solution of the Lindblad equation in the long-time limit.

Following Ref. [35] and Appendix A 3, the Liouvillian can be rewritten as

$$\mathcal{L} = \begin{pmatrix} \mathbf{c}' & \mathbf{c} \end{pmatrix} \begin{pmatrix} -X^T & Y \\ 0 & -X \end{pmatrix} \begin{pmatrix} \mathbf{c} \\ \mathbf{c}' \end{pmatrix}. \quad (21)$$

Here $\mathbf{c} = (c_{0,1} \cdots, c_{0,n}, c_{1,1} \cdots, c_{1,n})^T$ and $\mathbf{c}' = (c'_{0,1} \cdots, c'_{0,n}, c'_{1,1} \cdots, c'_{1,n})^T$ are the transformed bosonic operators. We define the following $2n \times 2n$ matrices

$$X = \begin{pmatrix} -A^* & B \\ -B^* & A \end{pmatrix} + \frac{i}{2} \begin{pmatrix} M - N^* & L^T - L \\ L^{\dagger} - L^* & M^* - N \end{pmatrix}, \quad (22)$$

$$Y = \frac{i}{2} \begin{pmatrix} -2iB^* - L^* - L^{\dagger} & 2N \\ 2N^T & 2iB - L - L^T \end{pmatrix}. \quad (23)$$

Here we define three $n \times n$ matrices

$$M_{ij} = \sum_{\mu} l_{\mu i} l_{\mu j}^*, \quad N_{ij} = \sum_{\mu} k_{\mu i} k_{\mu j}^*, \quad L_{ij} = \sum_{\mu} l_{\mu i} k_{\mu j}^*. \quad (24)$$

Ref. [34] proposed that the effective-Hamiltonian X in the open quantum system may play the role of the Hamiltonian in the corresponding isolated system. In general, X is a non-Hermitian matrix. Its $2n$ complex eigenvalues $\lambda_1, \cdots, \lambda_{2n}$ are the counterpart of the eigen-energies of the Hamiltonian of an isolated system.

Following the idea of Ref. [34], we can also use the three types of discrete symmetries to classify the effective Hamiltonian X from the Lindblad equation modeling a bosonic system influenced by the environment. For reasons that will be explained shortly, we decompose the effective Hamiltonian as

$$X = X_0 + X_1 = \begin{pmatrix} -A^* & B \\ -B^* & A \end{pmatrix} + \frac{i}{2} \begin{pmatrix} M - N^* & L^T - L \\ L^{\dagger} - L^* & M^* - N \end{pmatrix}. \quad (25)$$

The Hamiltonian part gives X_0 and the jump operator part gives X_1 . In what follows, we will first discuss the time-reversal symmetry. The key step is that the linear Lindblad operator satisfies

$$\mathcal{T}_S L_{\mu}^* \mathcal{T}_S^{\dagger} = L_{\mu}. \quad (26)$$

Here \mathcal{T}_S is the time-reversal operator applying to the system only. Recall that the boson operators transform under time reversal as

$$\mathcal{T}_S c_i \mathcal{T}_S^{\dagger} = \sum_j (T_S)_{ji}^* c_j, \quad \mathcal{T}_S c_i^{\dagger} \mathcal{T}_S^{\dagger} = \sum_j (T_S)_{ji} c_j^{\dagger}. \quad (27)$$

This leads to the following relations

$$\sum_i (T_S)_{ij}^* l_{\mu,j}^* = k_{\mu,i}, \quad \sum_i (T_S)_{ij} k_{\mu,j}^* = l_{\mu,i}, \quad (28)$$

which in turn determine the transformations of the matrices M , N and L as

$$T_S M T_S^{\dagger} = N^T, \quad T_S^* N T_S^T = M^T, \quad C_S L C_S^T = L^T \quad (29)$$

Note that both M and N are Hermitian matrices. Then the time-reversal of the jump operator part X_1 is

$$T X_1 T^{\dagger} = -X_1, \quad (30)$$

$$T = \begin{pmatrix} T_S & 0 \\ 0 & T_S^* \end{pmatrix}, \quad X_1 = \frac{i}{2} \begin{pmatrix} M - N^* & L^T - L \\ L^{\dagger} - L^* & M^* - N \end{pmatrix} \quad (31)$$

The Hamiltonian part X_0 is similar to the dynamic matrix H_{dyn} , which satisfies the ordinary time-reversal symmetry condition $T X_0^* T^{\dagger} = X_0$. If we assume the coefficients $l_{\mu,i}$ and $k_{\mu,i}$ in the jump operators are all real numbers, it follows that the jump operator part X_1 also satisfies $T X_1^* T^{\dagger} = X_1$. Combining these results, we arrived at $T X^* T^{\dagger} = X$. Therefore, in an open bosonic system described by the Lindblad equation, the time-reversal symmetry condition is applied to the complex conjugate of the effective Hamiltonian X , similar to the case of a fermionic Hamiltonian. However, this is different from the fermionic effective Hamiltonian of the Lindblad equation, where the time-reversal condition is applied to the transpose of the effective Hamiltonian [34].

Now we turn to the particle-hole symmetry. Since X is from the dynamic equation of ρ , we expect its symmetry transformations to be similar to those of H_{dyn} from the equation of motion rather than the Hermitian bosonic Hamiltonian H . Explicitly, the transformation matrix for the particle-hole symmetry can be taken as $C = \tau_1$, leading to

$$\tau_1 X_0^* \tau_1 = -X_0, \quad \tau_1 X_1^* \tau_1 = -X_1. \quad (32)$$

Therefore, we arrived at the particle-hole symmetry condition $\tau_1 X^* \tau_1 = -X$, which is the same as the quadratic fermionic model. The composition of the time-reversal and particle symmetries gives rise to the chiral symmetry condition $(CT)X(CT)^{\dagger} = -X$, which is also the same as the fermionic case. In summary, for the non-Hermitian

effective Hamiltonian X , the three discrete symmetry conditions are

$$\text{Time-reversal : } TX^*T^\dagger = X, TT^* = \pm 1, \quad (33)$$

$$\text{Particle-hole : } CX^*C^\dagger = -X, CC^* = \pm 1, \quad (34)$$

$$\text{Chiral or sublattice : } SX S^\dagger = -X, S^2 = 1. \quad (35)$$

Since the symmetry conditions are the same as the quadratic fermionic case, the ten-fold way classifications of quadratic fermionic systems [1] can also be applied to the effective Hamiltonian X of quadratic boson systems described by the Lindblad equation with linear Lindblad operators. Therefore, the classification produces the same table as Table I. However, the system-reservoir coupling in the Lindblad equation may lead to an explicit non-Hermitian effective Hamiltonian, causing subtle differences between the same model with and without the coupling to a reservoir.

Before demonstrating the subtle differences in the different classifying schemes by examples, we comment on the physical relevance of the schemes. For a closed bosonic system, the spectrum is determined by the dynamic matrix from the equation of motion or BdG diagonalization, so the classification follows Table I. The quasi-particle states may be used to determine the properties in this case. Since topological properties usually involve dynamic changes of the system [1, 2], the classification according to the dynamic matrix is common if the system is isolated. If the bosonic system is influenced by an environment and describable by the Lindblad formalism, the classification also follows Table I when one focuses on the effective behavior of the system. The properties may be extracted from the density matrix and its spectrum from the Lindblad equation, which incorporates the effects from the environment.

III. EXAMPLES

A. 1D bosonic pairing model

Our example to contrast the different classifications is a 1D bosonic pairing model inspired by the fermionic Kitaev chain [37]. Since the wavefunction is symmetric for bosons, we can have s-wave and d-wave pairing in the bosonic model rather than the p-wave pairing for spin-polarized fermion superconductors. The Hamiltonian of the 1D bosonic pairing model in real space is given by

$$H = \sum_i \left[iw(a_i^\dagger a_{i+1} + a_{i+1}^\dagger a_i) + \Delta_1 [(a_i^\dagger)^2 + a_i^2] + \Delta_2 (a_i^\dagger a_{i+1}^\dagger + a_{i+1} a_i) \right]. \quad (36)$$

Here a_i and a_i^\dagger are the annihilation and creation operators of bosons on site i . $\Delta_{1,2}$ denote the onsite and nearest-neighbor pairing, respectively. There have been studies on the bosonic analogues of the fermionic

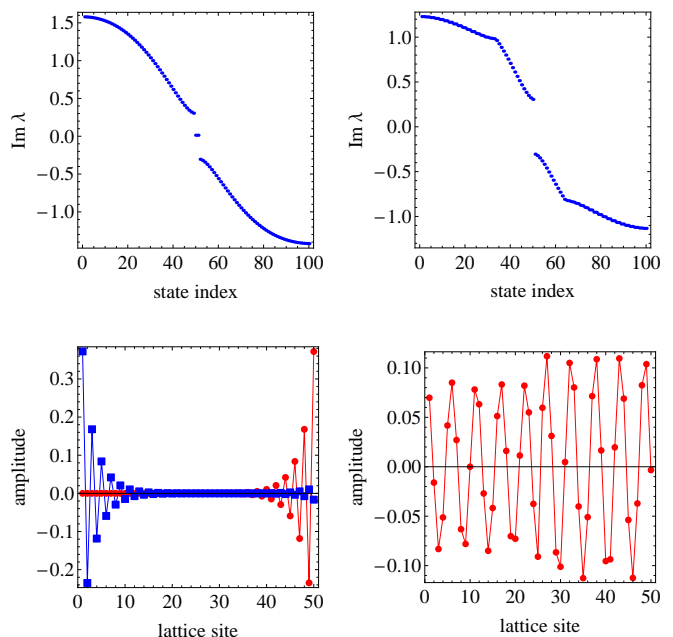


Figure 1. (Top row) Spectrum of the effective Hamiltonian of the 1D bosonic pairing model with open boundary condition for $\Delta_2 = 0.9$ (left) and $\Delta_2 = 0.3$ (right). Here $w = 1$, $\Delta_1 = 0.6$ and $\gamma = 0.2$. (Bottom row) Wave functions of the edge states (left) and a bulk state (right) on a finite lattice of 50 sites.

Kitaev model [14, 40–42] with pairing between neighbors, and here we study the model with both onsite and nearest-neighbor pairings in closed- and open-system settings. We mention the Hermitian Hamiltonian of the 1D bosonic pairing model alone does not imply nontrivial topological properties according to the result shown in the Appendix. In contrast, the Hamiltonian of the 1D fermionic Kitaev model already exhibits topological properties. Moreover, there are some subtleties in the classification of the fermion Kitaev chain, leading to different interpretations [1, 34] as summarized in the Appendix.

In order to find nontrivial topology of the 1D bosonic pairing model according to Table I, we have introduced a purely imaginary hopping coefficient similar to that used in Ref. [42]. Moreover, the bosons do not carry charge. The model may be realized using photonic simulators similar to that discussed in Ref. [42] or cold-atom simulators that can tune the hopping and interactions between bosons [43]. For the 1D bosonic pairing model, the classifications according to the dynamic matrix and the effective Hamiltonian are the same if the Lindblad operators do not break the particle-hole symmetry of the dynamic matrix. For example, we choose the Lindblad operators as

$$L_i = \gamma(a_i + a_{i+1}). \quad (37)$$

In momentum space, we define the "Nambu spinor" for bosons as $\psi = (a_k, a_{-k}^\dagger)^T$. The effective Hamiltonian

from the Lindblad equation is given by

$$X = \begin{pmatrix} -iw \sin k & \Delta_1 + \Delta_2 \cos k \\ -(\Delta_1 + \Delta_2 \cos k) & iw \sin k \end{pmatrix} + \frac{i}{2} \begin{pmatrix} 2\gamma^2(1 + \cos k) & 0 \\ 0 & 2\gamma^2(1 + \cos k) \end{pmatrix}. \quad (38)$$

The spectrum of the model is given by

$$\lambda = \pm i\sqrt{w^2 \sin^2 k + (\Delta_1 + \Delta_2 \cos k)^2} + i\gamma^2(1 + \cos k). \quad (39)$$

The topology of this model is characterised by the Berry phase, which is defined for a system with periodic boundary condition as

$$\theta = \int_0^{2\pi} dk \langle u_1 | \frac{\partial}{\partial k} | u_1 \rangle. \quad (40)$$

Here $|u_1\rangle$ is the eigenstate with $\text{Im}\lambda_1 < 0$. For the above model, we find that

$$\theta = \begin{cases} \pi, & \Delta_1 < \Delta_2, \\ 0, & \Delta_1 > \Delta_2. \end{cases} \quad (41)$$

Next, we will study the system with open boundary condition.

For the 1D bosonic pairing model with open boundary condition, we plot the imaginary part of the spectrum of the effective Hamiltonian in the top row of Figure 1 for $\Delta_2 = 0.9$, $\Delta_2 = 0.3$ and $\gamma = 0.2$, respectively. Both spectra are gapped, but there are two in-gap states connecting the two bands in the upper-left panel. In contrast, there is no in-gap state in the upper-right panel. Those in-gap states are localized edge states, as shown in the lower-left panel of Figure 1. To contrast the wavefunction profiles, we also plot the wavefunction of a typical bulk state showing no localization. The in-gap edge states emerge in the regime where the Berry phase takes the nontrivial value $\theta = \pi$. When $\theta = 0$, the system is topologically trivial and there is no localized edge state.

It can be verified that X respects particle hole symmetry because

$$\tau_1 X^*(-k) \tau_1 = -X(k). \quad (42)$$

Here τ_1 is the first Pauli matrix applying to the Nambu spinor space. Therefore, the effective Hamiltonian of the 1D bosonic pairing model belongs to class D of Table I, which supports a \mathbb{Z}_2 classification in 1D. If some perturbations are applied to the system while the particle-hole symmetry remains intact, we find that a pair of localized states at one end can merge together to acquire some non-zero eigen-energies. Because of this, the number of edge states is not conserved, but the parity of the number of edge states remains the same as long as the particle-hole symmetry is present. Therefore, the topologically nontrivial (trivial) phase corresponds to an odd (even) number of edge states at one end of the chain. We recall

that the Berry phase θ is an angle that is defined modulo 2π . This is consistent with the \mathbb{Z}_2 classification according to the Berry phase or the parity of the number of edge states.

In the example, the effective Hamiltonian and the dynamic matrix belong to the same symmetry class. One can change the effective Hamiltonian by using a different set of Lindblad operators. To demonstrate the possibility of having the dynamic matrix and effective Hamiltonian in different classes, we consider the Lindblad operators

$$L_j = \gamma(a_j - ia_{j+1}). \quad (43)$$

Note that for a time-reversal invariant system, we should impose the condition that the coefficients of the Lindblad operators are real numbers. However, the 1D bosonic pairing model does not have time-reversal symmetry. Therefore, we are allowed to use complex numbers in the example. In momentum space, the effective Hamiltonian is given by

$$X = H_{\text{dyn}} + \frac{i}{2} \begin{pmatrix} 2\gamma^2(1 + \sin k) & 0 \\ 0 & 2\gamma^2(1 + \sin k) \end{pmatrix}. \quad (44)$$

It can be shown that $\tau_1 X^*(-k) \tau_1 \neq -X(k)$, so the Lindblad operators break the particle-hole symmetry in X even though H_{dyn} respects the symmetry. As a consequence, X belongs to the class A, which is topologically trivial in 1D and different from the classification according to H_{dyn} .

We would like to mention that effects of spontaneously symmetry breaking on topological systems have been studied in Ref. [44]. Spontaneous symmetry breaking means the ground state of a system does not respect a symmetry of the Hamiltonian. In our classifications of bosonic systems, we analyze the symmetries of the Hamiltonian or its counterpart in open quantum systems. Therefore, the classifications do not take into consideration the broken symmetry in the ground state. Nevertheless, adding an explicitly symmetry-breaking term to the Hamiltonian or its counterpart in an open system may change its symmetry classification and cause different topological behavior. We remark that there exist examples [44] where the topology remains the same even though the ground states have different symmetries. Our discussions do not exclude those possibilities.

B. 2D Chern insulator

Next, we give an example that does not differentiate the three classifications of bosons. The example is a 2D model in class A without any symmetry, which can be thought of as the bosonic counterpart of the fermionic Chern insulator. In real space, the Hamiltonian is given

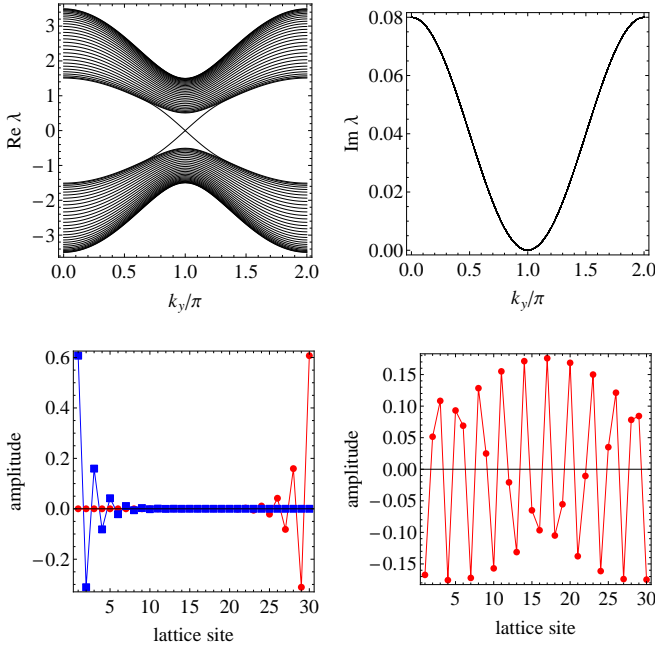


Figure 2. The top row shows the real (left) and imaginary (right) parts of the spectrum of the effective Hamiltonian of the 2D bosonic Chern insulator as a function of k_y for $m = 1.5$ and $\gamma = 0.2$. The bottom row shows the wave functions of the two edge states (left) and a typical bulk state (right) along the direction with open boundary condition.

by

$$\mathcal{H} = \sum_n \left(a_n^\dagger \frac{\sigma_3 - i\sigma_1}{2} a_{n+\hat{x}} + a_n^\dagger \frac{\sigma_3 - i\sigma_2}{2} a_{n+\hat{y}} + h.c. \right) + \sum_n m a_{n,s}^\dagger \sigma_3 a_n. \quad (45)$$

Here $n = (n_x, n_y)$ labels the lattice site on a square lattice. With two orbitals labelled by 1, 2 on each site, the boson operator is defined as $a_n = (a_{n,1}, a_{n,2})^T$. We also define \hat{x} and \hat{y} as the unit vectors along the x and y directions, respectively. There have been studies of the bosonic Chern insulator [8, 10], but here we analyze the model in both closed- and open- system settings. We remark that there is practically no difference between the bosonic and fermionic Chern insulators because the Chern insulator does not have any of the three classifying symmetries. Hence, the complication from the commutation and anticommutation relations does not play a significant role here. As a consequence, there is no difference among the three classifications for the 2D bosonic Chern insulator. Nevertheless, here we present the topological properties of the 2D bosonic Chern insulator described by the Lindblad equation.

The Lindblad operators we considered here have the form

$$L_{n,i} = \gamma(a_{n,i} + a_{n+\hat{y},i}) \quad \text{for } i = 1, 2. \quad (46)$$

Transforming the expression to momentum space, the effective Hamiltonian is given by

$$X = \begin{pmatrix} -H^* + iM/2 & 0 \\ 0 & H + iM^*/2 \end{pmatrix}. \quad (47)$$

The matrices H and M are defined by

$$H = \sum_{j=1}^3 R_j \sigma_j, \quad M = 2\gamma^2(1 + \cos k_y) I_0, \quad (48)$$

$$R_1 = \sin k_x, \quad R_2 = \sin k_y, \quad R_3 = m + \cos k_x + \cos k_y. \quad (49)$$

Here σ_j with $j = 1, 2, 3$ are the Pauli matrices and I_0 is the 2×2 identity matrix. The energy spectrum of the effective Hamiltonian is given by

$$\lambda = \pm \sqrt{R_1^2 + R_2^2 + R_3^2} + i\gamma^2(1 + \cos k_y). \quad (50)$$

The topology of this model may be characterized by the Chern number from the effective Hamiltonian. For the lower band, the Chern number can be related to the 2D winding number as

$$C = -\frac{1}{4\pi} \int d^2k \epsilon_{ijk} \hat{R}_i \cdot (\partial_x \hat{R}_j \times \partial_y \hat{R}_k). \quad (51)$$

For the 2D bosonic model discussed here, the Chern number takes the following values:

$$C = \begin{cases} 1, & 0 < m < 2, \\ -1, & -2 < m < 0, \\ 0, & |m| > 2. \end{cases} \quad (52)$$

For non-Hermitian models, one may introduce more types of topological invariants, such as the vorticity in the energy spectrum [23], defined as

$$v_n = \frac{1}{2\pi} \oint \nabla_{\mathbf{k}} \arg [\lambda_n(\mathbf{k})] \cdot d\mathbf{k}. \quad (53)$$

The vorticity counts the number of exceptional points inside the contour, and it is associated with the complex point gap [36, 45–47]. For the model studied here, however, the contribution from the system-reservoir coupling to the effective Hamiltonian of the Lindblad equation, M , is proportional to the identity matrix due to the choice of the Lindblad operators. Thus, there is no exceptional point, and the vorticity is trivial. For the discussion of Table I, it is more suitable to use the Chern number to characterize the topology. Nevertheless, one can see that this analysis offers another example that different topological classifications can be characterized by different physical quantities.

The Chern number is defined for systems with periodic boundary condition. We further consider the model on a cylinder-shape lattice. Explicitly, we impose open boundary condition along the x axis and periodic boundary condition along the y axis. The resulting Hamiltonian and effective Hamiltonian are still a function of k_y . In

Figure 2, we plot the eigenvalue spectrum of the effective Hamiltonian H_{eff} as a function of k_y . We have assumed $m = 1.5$, which corresponds to $C = 1$. In the upper left panel, one can see that there are two chiral edge states connecting the two bands. The edge states are localized at the two open ends of the cylinder. Moreover, there is no non-Hermitian skin effects because the non-Hermitian terms are diagonal. The typical profiles of the edge and bulk states are shown in the bottom of Figure 2. We remark that the system with $C = 0$ in the same cylinder geometry shows no chiral edge state.

C. 2D time-reversal invariant topological insulator

As another example, we consider the 2D time-reversal invariant topological insulator described by the four-band Bernevig-Hughes-Zhang (BHZ) model [38]. The bosonic BHZ model as an isolated system has been discussed in Ref. [7], and here we will further generalize it to include the environmental coupling. For experimental realization, we consider spin-1 bosonic atoms with the $S_z = 0$ component projected out [48]. The corresponding bosonic fields are $\psi = (\psi_{1\uparrow}, \psi_{2\uparrow}, \psi_{1\downarrow}, \psi_{2\downarrow})^T$, where the index $i = 1, 2$ labels the two orbitals and the up or down arrow labels $S_z = \pm 1$. The Hamiltonian of the BHZ model is given by

$$H_{\text{BHZ}} = \begin{pmatrix} H_0(\mathbf{k}) & H_1 \\ H_1^\dagger & H_0^*(-\mathbf{k}) \end{pmatrix}. \quad (54)$$

The H_0 term is a two-band Chern insulator considered in the previous subsection with the following expression

$$H_0 = \sin k_x \sigma_1 + \sin k_y \sigma_2 + (m + \cos k_x + \cos k_y) \sigma_3 \quad (55)$$

Here σ_i for $i = 1, 2, 3$ are the Pauli matrices. The H_1 term is given by

$$H_1 = \begin{pmatrix} 0 & \gamma \\ -\gamma & 0 \end{pmatrix}, \quad (56)$$

which couples the two spin components. It breaks the S_z conservation and the inversion symmetry, thereby making the model more generic. We remark that the BHZ model is not of the BdG form, so its dynamic matrix and Hamiltonian react to the time-reversal, particle-hole, and chiral symmetries in a similar fashion. Since the $S_z = \pm 1$ states correspond to a time-reversal pair, the time-reversal operator is given by $U_T K$ with $U_T = i\sigma_2$ and K denoting the complex conjugation. It follows that

$$U_T^\dagger H^*(\mathbf{k}) U_T = H(-\mathbf{k}). \quad (57)$$

Thus, the bosonic BHZ model belongs to the AII class with a \mathbb{Z}_2 topological index protected by the time-reversal symmetry similar to its fermionic counterpart.

For the BHZ model, the topological index is the Fu-Kane invariant [49] that can be constructed from the matrix W with the following elements

$$W_{ij}(\mathbf{k}) = \langle u_i(-\mathbf{k}) | U_T K | u_j(\mathbf{k}) \rangle. \quad (58)$$

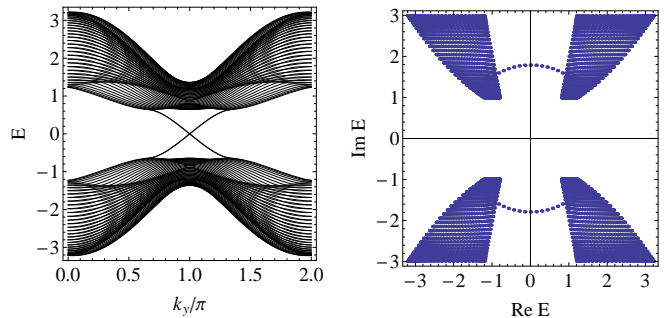


Figure 3. (Left) Band structure of the BHZ model described by Eq. (54) with $m = 1.2$ and $\gamma = 0.2$. (Right) Complex eigen-energy spectrum of the effective Hamiltonian given by Eq. (62) with $m = 1.2$, $\gamma = 0.2$, $g_1 = 2$, and $g_2 = 1$.

Here $|u_i(\mathbf{k})\rangle$ denotes the eigenstate in momentum space and the indices i, j run through all the occupied bands. W is an anti-symmetric matrix at the time reversal invariant momentum points $\mathbf{k}_1 = 0$, $\mathbf{k}_2 = (\pm\pi, 0)$, $\mathbf{k}_3 = (0, \pm\pi)$, and $\mathbf{k}_4 = (\pm\pi, \pm\pi)$. The Fu-Kane index can be obtained from the expression

$$I_{FK} = \prod_{i=1}^4 \frac{\text{Pf}[W(\mathbf{k}_i)]}{\sqrt{\det W(\mathbf{k}_i)}}. \quad (59)$$

Here the product runs through all the time reversal invariant momentum points, and ‘‘Pf’’ denotes the Pfaffian. For the BHZ model with small γ , the Fu-Kane invariant takes the values

$$I_{FK} = \begin{cases} -1, & |m| < 2, \\ 1, & |m| > 2. \end{cases} \quad (60)$$

The topology of the BHZ model can also be inferred from the edge modes when the system has open boundary condition. When the BHZ model is placed on a cylindrical lattice with open boundary along the x direction, its energy eigenvalues as a function of k_y are shown in the left panel of Figure 3. Here we assume $m = 1.2$ and $\gamma = 0.2$ in the topological regime. One can clearly see the edge modes corresponding to the non-trivial Fu-Kane invariant.

When the BHZ model is connected to a reservoir, we use the Lindblad equation to describe the open quantum system and first consider the following Lindblad operators

$$L_{n,i,\uparrow} = \gamma_1 a_{n,i,\uparrow} + \gamma_2 a_{n+\hat{x},i,\uparrow} \quad \text{for } i = 1, 2. \quad (61)$$

Since we only impose Lindblad operators for the spin-up bosons, it clearly breaks the time-reversal invariance. The effective Hamiltonian from the Lindblad equation thus belongs to the A class and describes a non-Hermitian Chern insulator. Transforming to momentum space, the effective Hamiltonian with periodic boundary condition

is given by

$$X = \begin{pmatrix} -H_{BHZ}^* + iM/2 & 0 \\ 0 & H_{BHZ} + iM^*/2 \end{pmatrix}. \quad (62)$$

where M is given by

$$M = 2 \begin{pmatrix} g_1 + g_2 \cos k_x & 0 \\ 0 & -(g_1 + g_2 \cos k_x) \end{pmatrix}. \quad (63)$$

Here $g_{1,2}$ depend on $\gamma_{1,2}$, but it is more convenient to treat them as tunable parameters. We have also subtracted a constant matrix in order to make M more symmetric.

The appearance of the $iM/2$ term provides an imaginary part for the eigen-energy. We plot the complex eigen-energy spectrum of the effective Hamiltonian with a cylindrical geometry in the right panel of Figure 3. In the original BHZ model, the bands of spin-up and spin-down bosons are nearly degenerate. With the Lindblad operators, the bands of the spin-up and spin-down bosons are separated by a finite imaginary part. The separation makes it possible to compute the Chern number for each band even when the eigenvalues are complex numbers. Our numerical calculations show that the two bands with positive real parts have $C = 1$ while the other two bands have $C = -1$. In the right panel of Figure 3, one can see that there exist edge modes between those bands for the BHZ model in a cylinder geometry. Therefore, the Lindblad operators turn the open-system BHZ model into an ordinary Chern insulator by breaking the time-reversal symmetry, characterized by a different topological index when compared to the isolated BHZ model.

IV. CONCLUSION

Depending on the different quantities used in the analyses, quadratic bosonic systems may fall into different topological classes with different interpretations. The non-Hermitian dynamic matrix is from the bosonic commutation relations and equation of motion, but there is no such complications in fermionic systems with the anticommutation relations. Although the classification tables according to the dynamic matrix of closed system and the effective Hamiltonian from the Lindblad equation of open system according to the three symmetries are the same, the Lindblad operators may change the symmetry properties and cause a model to be assigned to a different class compared to its closed-system counterpart. Our examples have demonstrated the subtle differences in topological properties according to the different settings and spin statistics. Realizations of the models in physical systems or quantum simulators will illustrate the rich physics of topological bosonic systems.

ACKNOWLEDGMENTS

Y. H. was supported by the Natural Science Foundation of China under Grant No. 11874272 and Science Specialty Program of Sichuan University under Grant No. 2020SCUNL210. C. C. C. was supported by the National Science Foundation under Grant No. PHY-2011360.

Appendix A: Some details

1. Classification of bosons according to the Hamiltonian

It is possible [18] to classify the Hermitian BdG Hamiltonian H by treating it as a mapping from the parameter space to a target space. However, our results summarized in Table II are different from those of Ref. [18], and the difference will be explained after we analyze the influence of the symmetries on the Hamiltonian. From Eqs. (2) and (3), the conditions of time-reversal and particle-hole symmetries are of the same form for boson systems. Actually, both of them impose a reality condition on the Hamiltonian. In the group-theory language, if the reality condition is not satisfied, the Hamiltonian is in a complex representation. If the reality condition is satisfied, the Hamiltonian is in a real or pseudo-real representation, corresponding to $T^*T = \pm 1$. Those three types of representations are equivalent to the class A (no time-reversal symmetry), class AI (time-reversal symmetry with $TT^* = 1$) and class AII (time-reversal symmetry with $TT^* = -1$) in Cartan's category. The three classes of Hamiltonians can also be represented by Hermitian complex, symmetric real, and Hermitian quaternion matrices, respectively. We remark that the classification of the three types of representations is independent of the basis. Therefore, if there are two reality conditions, they must be compatible with each other. When both conditions are present, they determine the same symmetry class as only one reality condition.

Now we turn to the chiral symmetry of bosonic Hamiltonians. The chiral symmetry (4) means that there is a matrix S that commutes with the Hamiltonian. This implies that one can find a non-trivial invariant space in the total Hilbert space, or the Hamiltonian can be put into a block-diagonal form. Therefore, we can focus on only one block, where there is no chiral symmetry any more. In other words, the chiral symmetry of bosonic systems will not change the symmetry class. This is in contrast with the chiral symmetry of fermionic systems, which has an anti-commutation relation with the Hamiltonian.

After clarifying the three types of symmetry conditions, we proceed to analyze the topological classes according to these symmetries. First, if there is no symmetries, the Hamiltonian is a Hermitian complex matrix, which can be labeled as class C. We can impose a chiral symmetry on class C without imposing any reality

Class	T	C	S	$d=0$	$d=1$	$d=2$	$d=3$	$d=4$	$d=5$	$d=6$
C	0	0	0	\mathbb{Z}	0	\mathbb{Z}	0	\mathbb{Z}	0	\mathbb{Z}
CI	0	0	1	\mathbb{Z}	0	\mathbb{Z}	0	\mathbb{Z}	0	\mathbb{Z}
R	+	0	0	\mathbb{Z}	0	0	0	\mathbb{Z}	0	\mathbb{Z}_2
RI	0	+	0	\mathbb{Z}	0	0	0	\mathbb{Z}	0	\mathbb{Z}_2
RII	+	+	1	\mathbb{Z}	0	0	0	\mathbb{Z}	0	\mathbb{Z}_2
H	-	0	0	\mathbb{Z}	0	\mathbb{Z}_2	\mathbb{Z}_2	\mathbb{Z}	0	0
HI	0	-	0	\mathbb{Z}	0	\mathbb{Z}_2	\mathbb{Z}_2	\mathbb{Z}	0	0
HII	-	-	1	\mathbb{Z}	0	\mathbb{Z}_2	\mathbb{Z}_2	\mathbb{Z}	0	0

Table II. Classification of quadratic bosonic systems according to their Hamiltonians. The first column shows the labels of the classes. The next three columns show the properties of the classes under time-reversal, particle-hole, and chiral symmetries. Here 0 or 1 represents the absence or presence of the symmetry. The + and - signs correspond to $TT^* = \pm 1$ and $CC^* = \pm 1$. The last seven columns show the possible topological phases of the eight classes in different dimensions.

conditions. This class can be labeled as CI. Both C and CI class have the same classifying space $\mathcal{C}_0 = \mathbb{Z} \times BU$. From this, we obtain the first two rows of Table II. Following class C, we can impose time-reversal symmetry with $T^*T = 1$, particle-hole symmetry with $C^*C = 1$, or both. The three classes are labeled as R, RI, and RII since they all contain real matrices. They also have the same classifying space $\mathcal{R}_0 = \mathbb{Z} \times BO$, from which one can derive the third to fifth rows of Table II. Similarly, one can also impose time-reversal symmetry with $T^*T = -1$, particle-hole symmetry with $C^*C = -1$, or both, which correspond to classes H, HI, and HII containing Hermitian quaternion matrices. The three also have the same classifying space $\mathcal{R}_4 = \mathbb{Z} \times BSp$, giving rise to the last three rows of Table II. The "three-fold way" thus refers to the three distinct classifying spaces. We remark that due to the same reality conditions from time-reversal and particle-hole symmetries on bosonic Hamiltonians, the classification of Table II is different from the results of Ref. [18], which did not fully discern the consequences from the two symmetries.

We also give a more detailed account for the differences between fermionic and bosonic systems. The particle-hole symmetry applies to the fermion creation and annihilation operators according to

$$\mathcal{C}\psi_a\mathcal{C}^{-1} = \sum_b C_{ab}^T \psi_b^\dagger. \quad (\text{A1})$$

Suppose the Hamiltonian in the second quantization form is given by Eq. (1), then the particle-hole symmetry requires that $\mathcal{H} = \mathcal{C}\mathcal{H}\mathcal{C}^{-1}$. Making use of the transformation of Eq. (A1), we find that

$$\begin{aligned} \mathcal{C}\mathcal{H}\mathcal{C}^{-1} &= \sum_{a,b,c,d} \psi_a C_{da}^* H_{ab} C_{bc}^T \psi_c^\dagger \\ &= - \sum_{a,b,c,d} \psi_c^\dagger C_{cb} H_{ba}^T C_{ad}^\dagger \psi_d + \text{constant}. \end{aligned} \quad (\text{A2})$$

In the second line, we have used the anti-commutation relations to switch the order of the fermion creation and annihilation operators, causing a minus sign. Comparing the above equation with \mathcal{H} , we arrived at the claimed particle-hole symmetry for the Hamiltonian in the first quantization form as $CH^*C^\dagger = -H$. The same procedure also applies to bosonic Hamiltonians, but the bosonic commutation relations should be used instead of the fermionic anti-commutation relations. Therefore, $CH^*C^\dagger = H$ without a minus sign for bosonic systems.

The absence of the minus sign for the particle-hole and chiral symmetries of bosonic Hamiltonians leads to a different classification when compared to the fermions. We first check the symmetry class A in the fermion ten-fold way classification in zero dimension. The class A has no symmetry, and there is no constraint on the class A Hamiltonian. If we impose chiral symmetry on the class A, we arrived at a new class AIII. The effect of chiral symmetry is to require that the Hamiltonian in class AIII anti-commutes with a certain matrix e_1 . If we treat the matrix e_1 as a basis vector of the Clifford algebra, the process of imposing the chiral symmetry is actually equivalent to the Clifford algebra extension $Cl_0 \rightarrow Cl_1$. Therefore, the classifying space of the class AIII is different from the class A. On the other hand, there is no minus sign in the relation of chiral symmetry for bosonic Hamiltonians. Imposing chiral symmetry only requires the Hamiltonian to commute with a certain matrix but does not change the classifying space. Therefore, the effects of particle-hole and chiral symmetries according to bosonic Hamiltonians, summarized in Table II, are different from those in fermionic systems following the ten-fold way table. In contrast, the particle-hole and chiral symmetries for the dynamic matrix and effective Hamiltonian of a bosonic system act similarly as their fermionic counterparts, leading to the classifications shown in Table I.

2. Dynamic matrix

If we try to diagonalize the Hermitian BdG Hamiltonian of bosons shown in Eq. (1) as

$$V^\dagger H V = \Lambda \quad (\text{A3})$$

with a diagonal matrix Λ , then the matrix V must satisfy

$$V^\dagger \tau_3 V = \tau_3 \quad (\text{A4})$$

in order to preserve the bosonic canonical commutation relations. The matrix V is actually a para-unitary matrix. We can rewrite Eq. (A3) as

$$V^{-1}(\tau_3 H)V = \tau_3 \Lambda. \quad (\text{A5})$$

The dynamic matrix then has the standard structure of the matrix diagonalization. Here the τ_3 factor compensates for the signature in the definition of the para-unitary matrix.

3. Third quantization of bosons

Following the method of Ref. [35], also known as the ‘‘third quantization’’, one can define a vector space \mathcal{K} that contains the trace class operators and a vector space \mathcal{K}' that contains the unbounded operators, such as physical observables. The elements in \mathcal{K} can be written as a ket $|\rho\rangle$ while the element in \mathcal{K}' can be written as a bra $\langle A|$. The inner product of these spaces is defined as $\langle A|\rho\rangle = \text{tr}(A\rho)$. For a boson operator a , we can define the following left- and right-multiplication maps in \mathcal{K} as follows.

$$a^L|\rho\rangle = |a\rho\rangle, \quad a^R|\rho\rangle = |\rho a\rangle. \quad (\text{A6})$$

According to the cyclic property of trace, these maps apply to \mathcal{K}' as follows.

$$\langle\rho|a^L = \langle\rho a|, \quad \langle\rho|a^R = \langle a\rho|. \quad (\text{A7})$$

In terms the above maps of \mathcal{K} , we can introduce $4n$ maps in the operator space as $c_{\nu,j}$ and $c'_{\nu,j}$ for $\nu = 0, 1$ and $j = 1, \dots, n$ as follows.

$$c_{0,j} = a_j^L, \quad c'_{0,j} = a_j^{\dagger L} - a_j^{\dagger R}, \quad c_{1,j} = a_j^{\dagger R}, \quad c'_{1,j} = a_j^R - a_j^L. \quad (\text{A8})$$

The definition of $c'_{\mu,j}$ is designed to right-annihilate the identity operator, $\langle 1|c'_{\mu,j} = 0$. One can verify that they satisfy the canonical commutation relations

$$[c_{\mu,i}, c'_{\nu,j}] = \delta_{\mu\nu}\delta_{ij}, \quad [c_{\mu,i}, c_{\nu,j}] = 0, \quad [c'_{\mu,i}, c'_{\nu,j}] = 0. \quad (\text{A9})$$

The super-operator \mathcal{L} in the Lindblad equation (18) may be rewritten as

$$\mathcal{L} = \mathcal{H}^L - \mathcal{H}^R + i \sum_{\mu} \left(2L_{\mu}^L L_{\mu}^{\dagger R} - L_{\mu}^{\dagger L} L_{\mu}^L - L_{\mu}^R L_{\mu}^{\dagger R} \right). \quad (\text{A10})$$

We want to express the above equation in terms of c and c' . To this ends, we reverse the definitions of c and c' and find

$$\begin{aligned} a_j^L &= c_{0,j}, & a_j^{\dagger L} &= c'_{0,j} + c_{1,j}, \\ a_j^R &= c_{0,j} + c'_{1,j}, & a_j^{\dagger R} &= c_{1,j}. \end{aligned} \quad (\text{A11})$$

Together with Eq. (19), it can be shown that

$$\begin{aligned} \mathcal{H}^L &= \sum_{ij} \left[2A_{ij}(c'_{0,i} + c_{1,i})c_{0,j} + B_{ij}c_{0,i}c_{0,j} \right. \\ &\quad \left. + B_{ij}^*(c'_{0,i} + c_{1,i})(c'_{0,j} + c_{1,j}) \right], \end{aligned} \quad (\text{A12})$$

$$\begin{aligned} \mathcal{H}^R &= \sum_{ij} \left[2A_{ij}c_{1,i}(c_{0,j} + c'_{1,j}) + B_{ij}^*c_{1,i}c_{1,j} \right. \\ &\quad \left. + B_{ij}(c_{0,i} + c'_{1,i})(c_{0,j} + c'_{1,j}) \right], \end{aligned} \quad (\text{A13})$$

and

$$L_{\mu}^L = \sum_j \left[l_{\mu j}c_{0,j} + k_{\mu,j}(c'_{0,j} + c_{1,j}) \right], \quad (\text{A14})$$

$$L_{\mu}^{\dagger L} = \sum_j \left[l_{\mu j}^*(c'_{0,j} + c_{1,j}) + k_{\mu,j}^*c_{0,j} \right], \quad (\text{A15})$$

$$L_{\mu}^R = \sum_j \left[l_{\mu j}(c_{0,j} + c'_{1,j}) + k_{\mu,j}c_{1,j} \right], \quad (\text{A16})$$

$$L_{\mu}^{\dagger R} = \sum_j \left[l_{\mu j}^*c_{1,j} + k_{\mu,j}^*(c_{0,j} + c'_{1,j}) \right]. \quad (\text{A17})$$

Applying the results to Eq. (A10), the super-operator \mathcal{L} is now in a quadratic form of c and c' . After some algebra, the final result can be found in Eq. (14) of Ref. [35]. Written in a matrix form, we arrived at Eq. (21).

4. Subtlety of fermionic Kitaev chain

The Hamiltonian of the fermionic Kitaev chain with p -wave pairing is given by

$$H = \sum_i \left[\mu c_i^{\dagger} c_i + w(c_i^{\dagger} c_{i+1} + h.c.) + \Delta(c_i^{\dagger} c_{i+1}^{\dagger} + h.c.) \right]. \quad (\text{A18})$$

Usually, the fermion Kitaev chain is considered to belong the class D [1]. But if we rewrite the Hamiltonian in terms of Majorana fermions defined as $c_j = a_{2j-1} + ia_{2j}$, then we find

$$\begin{aligned} H &= \frac{i}{2} \sum_j \left(\mu a_{2j-1} a_{2j} + (\Delta - w) a_{2j} a_{2j+1} \right. \\ &\quad \left. + (\Delta + w) a_{2j-1} a_{2j+2} \right). \end{aligned} \quad (\text{A19})$$

If we make transformations $a_{2j-1} \rightarrow a_{2j-1}$ and $a_{2j} \rightarrow -a_{2j}$, then the Hamiltonian gets a minus sign $H \rightarrow -H$. Therefore, in terms of Majorana fermions, this model also satisfies chiral symmetry and belong to the class BDI [34]. In 1D, class BDI has \mathbb{Z} classification. We caution that the difference is at the level of models because the ten-fold classification shown in Table I is based on the symmetries of the system.

-
- [1] C.-K. Chiu, J. C. Y. Teo, A. P. Schnyder, and S. Ryu, *Rev. Mod. Phys.* **88**, 035005 (2016).
- [2] T. D. Stanescu, *Introduction to topological quantum matter and quantum computation* (CRC Press, Boca Raton, FL, USA, 2017).
- [3] A. L. Fetter and J. D. Walecka, *Quantum Theory of Many-Particle Systems* (Dover Publications, Mineola, NY, 2003).
- [4] S. Ronen, D. C. E. Bortolotti, and J. L. Bohn, *Phys. Rev. A* **74**, 013623 (2006).
- [5] C. J. Pethick and H. Smith, *Bose-Einstein condensation in dilute gases* (Cambridge University Press, Cambridge, UK, 2008), 2nd ed.
- [6] S. Furukawa and M. Ueda, *New J. Phys.* **17**, 115014 (2015).
- [7] J. Wang, W. Zheng, and Y. Deng, *Phys. Rev. A* **102**, 043323 (2020).
- [8] V. Peano, M. Houde, C. Brendel, F. Marquardt, and A. A. Clerk, *Nat. Comm.* **7**, 10779 (2016).
- [9] C. Sanavio, V. Peano, and A. Xuereb, *Phys. Rev. B* **101**, 085108 (2020).
- [10] R. Shindou, R. Matsumoto, S. Murakami, and J. I. Ohe, *Phys. Rev. B* **87**, 174427 (2013).
- [11] M. Lein and K. Sato, *Phys. Rev. B* **100**, 075414 (2019).
- [12] H. Kondo, Y. Akagi, and H. Katsura, *Prog. Theor. Exp. Phys.* **2020**, 12A104 (2020).
- [13] S. Park and B. J. Yang, *Phys. Rev. B* **99**, 174435 (2019).
- [14] S. Lieu, *Phys. Rev. B* **98**, 115135 (2018).
- [15] J. Curtis, G. Refael, and V. Galitski, *Ann. Phys.* **407**, 148 (2019).
- [16] Y. Akagi, *J. Phys. Soc. Jpn.* **89**, 123601 (2020).
- [17] H. Y. Ling and B. Kain, *Selection rule for topological amplifiers in bogoliubov de gennes systems* (2021), arXiv: 2011.14935.
- [18] Z. Zhou, L. L. Wan, and Z. F. Xu, *J. Phys. A: Math. Theor.* **53**, 425203 (2020).
- [19] V. P. Flynn, E. Cobanera, and L. Viola, *New J. Phys.* **22**, 083004 (2020).
- [20] Q. R. Xu, V. P. Flynn, A. Alase, E. Cobanera, L. Viola, and G. Ortiz, *Phys. Rev. B* **102**, 125127 (2020).
- [21] Y. Ashida, Z. Gong, and M. Ueda, *Adv. Phys.* **69**, 249 (2021).
- [22] K. Yokomizo and S. Murakami, *Non-bloch band theory in bosonic bogoliubov-de gennes systems*, arXiv:2012.00439.
- [23] A. Ghatak and T. Das, *J. Phys.: Condens. Matter* **31**, 263001 (2019).
- [24] S. Haroche and J. M. Raimond, *Exploring the Quantum: Atoms, Cavities, and Photons* (Oxford University Press, Oxford, UK, 2006).
- [25] H. P. Breuer and F. Petruccione, *The theory of open quantum systems* (Oxford University Press, Oxford, UK, 2006).
- [26] U. Weiss, *Quantum Dissipative Systems* (World Scientific Publishing, Singapore, 2012), 4th ed.
- [27] S. Diehl, E. Rico, M. A. Baranov, and P. Zoller, *Nat. Phys.* **7**, 971 (2011).
- [28] Z. Huang and D. P. Arovas, *Phys. Rev. Lett.* **113**, 076407 (2014).
- [29] F. Song, S. Yao, and Z. Wang, *Phys. Rev. Lett.* **123**, 170401 (2019).
- [30] M. Asorey, P. Facchi, and G. Marmo, *Open Sys. and Inf. Dyn.* **26**, 1950012 (2019).
- [31] S. Bandyopadhyay, S. Bhattacharjee, and D. Sen, *Driven quantum many-body systems and out-of-equilibrium topology* (2021), arXiv: 2103.02279.
- [32] A. McDonald, R. Hanai, and A. A. Clerk, *Non-equilibrium stationary states of quantum non-hermitian lattice models* (2021), arXiv: 2103.01941.
- [33] T. Prosen, *New J. Phys.* **10**, 043026 (2008).
- [34] S. Lieu, M. McGinley, and N. R. Cooper, *Phys. Rev. Lett.* **124**, 040401 (2020).
- [35] T. Prosen and T. H. Seligman, *J. Phys. A: Math. Theor.* **43**, 392004 (2010).
- [36] K. Kawabata, K. Shiozaki, M. Ueda, , and M. Sato, *Phys. Rev. X* **9**, 041015 (2019).
- [37] A. Kitaev, *Annals of Physics* **321**, 2 (2006).
- [38] B. A. Bernevig, T. L. Hughes, and S.-C. Zhang, *Science* **314**, 1757 (2006).
- [39] M. Konig, S. Wiedmann, C. Brüne, A. Roth, H. Buhmann, L. W. Molenkamp, X.-L. Qi, and S.-C. Zhang, *Science* **318**, 766 (2007).
- [40] R. Barnett, *Phys. Rev. A* **88**, 063631 (2013).
- [41] G. Engelhardt, M. Benito, G. Platero, and T. Brandes, *Phys. Rev. Lett.* **117**, 045302 (2016).
- [42] A. McDonald, T. Pereg-Barnea, and A. A. Clerk, *Phys. Rev. X* **8**, 041031 (2018).
- [43] S. Vishveshwara and D. M. Weld, *Z2 phases and majorana spectroscopy in paired bose-hubbard chains* (2020), arXiv: 2012.02380.
- [44] A. Raj, N. Banerjee, and T. Das, *Phys. Rev. B* **103**, 075139 (2021).
- [45] H. Shen, B. Zhen, and L. Fu, *Phys. Rev. Lett.* **120**, 146402 (2018).
- [46] P. A. McClarty and J. G. Rau, *Phys. Rev. B* **100**, 100405(R) (2019).
- [47] E. J. Bergholtz, J. C. Budich, and F. K. Kunst, *Rev. Mod. Phys.* **93**, 015005 (2021).
- [48] D. M. Stamper-Kurn and M. Ueda, *Rev. Mod. Phys.* **85**, 1191 (2013).
- [49] L. Fu, C. L. Kane, and E. J. Mele, *Phys. Rev. Lett.* **98**, 106803 (2007).